Inorganic Chemistry
Article
pubs.acs.org/IC

Probing Highly Luminescent Europium-Doped Lanthanum Orthophosphate Nanorods for Strategic Applications

Mohit Saraf,[†,#] Pawan Kumar,[†,#] Garima Kedawat,[‡,○] Jaya Dwivedi,[†] Sajna Antony Vithayathil,[∥] Nagendra Jaiswal,[§] Benny Abraham Kaipparettu,[⊥,∥] and Bipin Kumar Gupta*[,†]

[†]CSIR-National Physical Laboratory, Dr K S Krishnan Road, New Delhi 110012, India

[‡]Department of Physics, University of Rajasthan, Jaipur 302055, India

[§]Advertising and Communication Printing Agency, Maldahiya, Varanasi, Uttar Pradesh 221006, India

[∥]Department of Molecular and Human Genetics and [⊥]Dan L. Duncan Cancer Center, Baylor College of Medicine, Houston, Texas 77030, United States

Supporting Information

ABSTRACT: Herein we have established a strategy for the synthesis of highly luminescent and biocompatible europium-doped lanthanum orthophosphate ($La_{0.85}PO_4Eu_{0.15}^{3+}$) nanorods. The structure and morphogenesis of these nanorods have been probed by XRD, SEM, and TEM/HRTEM techniques. The XRD result confirms that the as-synthesized nanorods form in a monazite phase with a monoclinic crystal structure. Furthermore, the surface morphology shows that the synthesized nanorods have an average diameter of ~90 nm and length of ~2 μm. The HRTEM images show clear lattice fringes that support the presence of better crystal quality and enhanced photoluminescence hypersensitive red emission at 610 nm ($^5D_0-^7F_2$) upon 394 nm wavelength excitation. Furthermore, time-resolved spectroscopy and an MTT assay of these luminescent nanorods demonstrate a photoluminescent decay time of milliseconds with nontoxic behavior. Hence, these obtained results suggest that the as-synthesized luminescent nanorods could be potentially used in invisible security ink and high-contrast bioimaging applications.

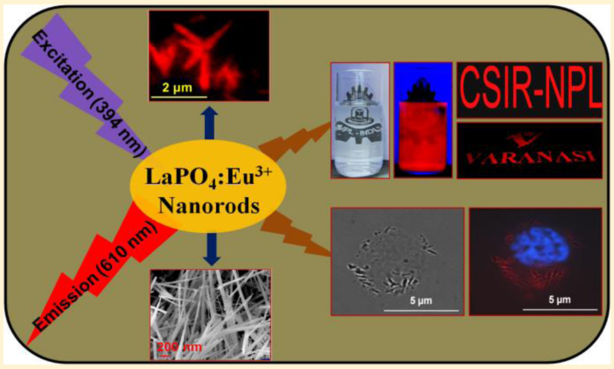

1. INTRODUCTION

Recently, the orthophosphate family has gained huge attention in a variety of applications that include optoelectronic devices, display devices, security inks, bioimaging, and biotagging owing to their intriguing size and shape-dependent properties.[1−9] In fact, it has been demonstrated that the physical and chemical properties of nanophosphate materials are strongly related to their size, morphology and crystallographic nature.[10,11] Significant research efforts have been carried out toward the synthesis of inorganic nanostructures with controlled shape, uniform narrow size distribution, and good morphologies, by virtue of their novel and striking properties.

The rare-earth-doped nanostructures have been recognized globally for their superior chemical and optical properties originating from their unique electronic structures.[12−23] In comparison to organic dyes, metals and metal oxides, semiconductor quantum dots such as CdS, CdSe, and CdTe,[7,8] and core−shell structures such as CdSe/ZnS, CdSe/CdS, and TiO_2/CdS,[24−26] rare-earth compounds such as lanthanides offer intense and narrow emission bands arising from f−f transitions and large Stokes shifts with the exclusion of particular drawbacks such as biotoxicity, low light penetration depth, and optical blinking.[27−36] It is well-known that the rare-earth ions with have an empty, half, or fully filled 4f electron shell configuration and these ions have capability of inducing the efficient generation of individual color emissions in multiphosphor devices. Currently, there have been intense investigations on lanthanide ions doped in inorganic host materials, (RE)PO_4 (RE = Y, La, Gd, Lu), as these possess beneficial properties[37] such as high refractive index ($n \approx 1.5$), high thermal stability (~2300 °C), high luminescence efficiency, flexible emission colors with different activators, low toxicity, and high photochemical stability. Lanthanum phosphate ($LaPO_4$) nanomaterials are very attractive benign fluorescent phosphors in comparison to traditional semiconductor quantum dots because of their luminescence in the presence of a suitable dopant such as europium ion (Eu^{3+}) in $LaPO_4$ nanowires, their high fluorescence quantum yield, and improved rate of radiative transitions.[38] The monophosphates or orthophosphates are structurally the simplest type of phosphates consisting of isolated PO_4 tetrahedrons. Each PO_4

Received: November 18, 2014
Published: March 2, 2015

DOI: 10.1021/ic5027784

tetrahedron shares one or more of its oxygen ions with neighboring tetrahedra to produce more complex phosphates. Such materials hold great promise in various applications, as the continuously linked tetrahedra can provide conduction pathways for transport of charge within these structures leading to extremely high conductivity. Continuously linked tetrahedra of PO_4 essentially provide an obstructionless expressway for the transport of protons through the structure.[39] It is important to generate a rare earth ion doped $LaPO_4$ host lattice ($LaPO_4$:Eu^{3+}) for the development of nanomaterials that are stable, intense, and nontoxic, have various color emissions with high quantum efficiencies, and can be used as biolabels for applications such as a red emitter in fluorescent lamps, cathode ray tubes, lighting, lasers, biological labels, and plasma display panels (PDPs). This lattice possesses excellent chemical and thermal stabilities as well, as it is a highly efficient phosphor with a quantum yield of >90%.[2−4] Additionally, recent reports on lanthanum phosphate demonstrate that it could be potentially dispersed in water for a transparent colloidal suspension, which is highly required for our proposed applications in the present studies.[40] Nanostructured $LaPO_4$ with controlled size and dimensions are thought to display novel size- and shape-dependent properties in comparison to bulk $LaPO_4$. For example, Eu^{3+}-doped $LaPO_4$ nanowires/nanorods exhibit high fluorescence quantum yields and enhanced radiative transition rates in comparison with their corresponding isotropic nanoparticles, microparticles, and microrods.[41,42]

Several research groups have reported the fabrication and assembly of various 1D nanostructures of $LaPO_4$ nanomaterials, such as nanowires, nanorods, and nanocables, using various synthetic routes. However, it is very cumbersome to understand the tedious synthesis mechanism taking place under such extreme conditions. Thus, the development of practical approaches for the synthesis of large quantities of low-cost 1D nanostructures is still a challenging task.[26]

In this article, we focus on the synthesis of red-emitting homogeneous $La_{0.85}PO_4Eu_{0.15}{}^{3+}$ nanorods by customized chemical precipitation. The optimization of concentration of activator europium (Eu^{3+}) ions incorporated into the host lattice during the synthesis of the phosphor nanorods is essential for developing highly luminescent Eu^{3+}-doped $LaPO_4$ nanorods as well as the growth of the rods. Our results reveal that the monazite crystalline phase of Eu^{3+}-doped $LaPO_4$ nanorods with a monoclinic crystal structure provides relatively long-lived hypersensitive red emissions at 610 nm upon 394 nm wavelength excitation (xenon lamp as the source of excitation). We also investigated transparent and water-stable luminescent Eu^{3+}-doped $LaPO_4$ colloids as invisible luminescent inks, which exhibited good colloidal stability with PVC gold medium (the composition of the PVC gold medium is polyvinyl chloride resin + cyclohexanone + nitrobenzene + ethyl cellulose + C_9 reducer (aromatic hydrocarbon solvent)) for several hours and a strong red emission peak at 610 nm upon 254 nm excitation with a portable UV lamp. This kind of ink is highly useful in data production and anticounterfeiting applications. The process of ink fabrication is facile and suitable for bulk production at an economical cost. However, there have been a few reports on security ink with isotropic nanoparticles with PVA (poly(vinyl alcohol)), sodium hexametaphosphate (SHMP), cyclohexane, and poly(methyl methacrylate) (PMMA)[9,43,44] but there have been no attempts to use a commercially available PVC gold medium, which acts here as a magic medium and has the capability of dispersing the phosphate materials in the medium. The nanorod structure plays an important role in fabricating the luminescent ink. The existing semiconductor nanoparticles (e.g., CdS, CdSe, CdTe, etc.) which are widely used to make security ink are toxic. The rare-earth $La_{0.85}PO_4Eu_{0.15}$ nanorods are easily dispersed into the PVC gold medium without formation of clusters or agglomerates of nanorods for invisible luminescent security ink applications. The additional advantage of the nanorod structure is used in this study because the nanorod shape acts as a better in-filler in cellulose-based PVC ink medium in comparison to other isotropic nanoparticles. Recently, we have established in previous studies the development of a rare earth oxide nanorod (Y_2O_3:Er^{3+}/Yb^{3+} nanorod) based security ink for anticounterfeiting applications.[45] In addition to this application, one-dimensional (1D) nanostructures of $LaPO_4$ are also alluring due to their striking possibility of deep penetration in biological cells and enhanced motion in cellular fluids along with the future prospect of healing action. Their biocompatibility or cytotoxicity primarily depends on their size as well as their molecular design.[46] The in vitro studies in HeLa cells using this kind of phosphate nanorod is reported, which clearly demonstrates the feasibility of nanorods in biological applications for cell labeling and cellular imaging.[46] Therefore, we have also demonstrated another strategic application of highly biocompatible $La_{0.85}PO_4Eu_{0.15}{}^{3+}$ nanorods as a biological nanoprobe for high-contrast in vitro cellular imaging studies of human breast cancer cells.

2. EXPERIMENTAL SECTION

2.1. Synthesis of $La_{1-x}PO_4$:$Eu_x{}^{3+}$ Nanorods. In the typical synthesis of $La_{1-x}PO_4Eu_x{}^{3+}$ (x = 0.05−0.50) nanorods, an efficient and customized method of chemical precipitation was used. The precursor materials La_2O_3 (99.99%), Eu_2O_3 (99.99%), HNO_3 (AR grade, 69%), phosphoric acid (H_3PO_4), and ammonium hydroxide (NH_4OH, GR grade) were procured from Sigma-Aldrich. For the synthesis of $La_{1-x}PO_4Eu_x{}^{3+}$ nanorods, the molar ratio is given in Table S1 (see the Supporting Information) for different concentrations of Eu in $La_{1-x}PO_4Eu_x{}^{3+}$. La_2O_3 and Eu_2O_3 with x = 0.15 molar ratio were mixed well in a beaker with a minimum quantity of deionized water. Since rare-earth oxides are insoluble in water, a few drops of concentrated HNO_3 were added to the solution with constant stirring at ∼100 °C for 2 h to dissolve it completely. The obtained milky white solution was turned into a transparent lanthanum and europium nitrate solution. Then, NH_4OH was added to the transparent nitrate solution to change the pH of the solution. The pH value plays a critical role in controlling the shape, size, and efficient luminescence of the synthesized product. This obtained solution was converted into the hydroxide intermediate structure using low and high pH values. This intermediate stage is responsible for designing the structure and shape of the final product. It can be noted that a lower pH value of the metal complex precursor controls the slow nucleation reaction and as a result isotropic nanoparticles forms The SEM image of the obtained product at pH ∼4 is shown in Figure S1 (see the Supporting Information). This image depicts spherical particles having the diameter ∼80 nm. However, at high pH, a fast and anisotropic nucleation reaction occurs and as a result nanorod-like structures were formed (see Figure S2 in the Supporting Information). Hereafter, this solution was treated with an appropriate quantity of H_3PO_4 acid to convert the hydroxide into phosphate and it was added drop by drop into the solution. The white precipitate was observed due to the formation of the metal complex $LaPO_4$. Our experimental observations suggest that when the final products change from hydroxide into phosphate, the surface morphology does not change. Lower pH produce isotropic nanoparticles (Figure S3; see the Supporting Information), while higher pH offer nanorod crystal structures (Figure S4; see the Supporting

DOI: 10.1021/ic5027784
Inorg. Chem. 2015, 54, 2616−2625

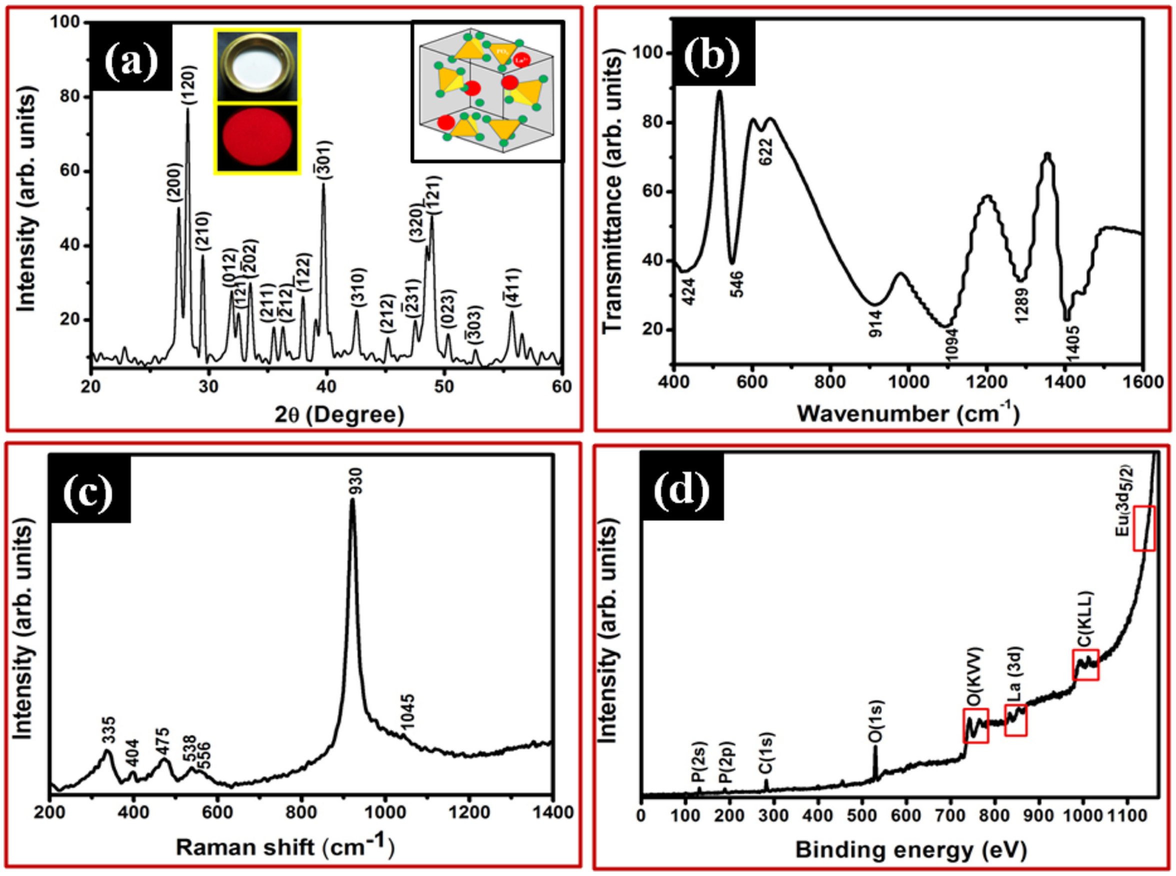

Figure 1. (a) XRD pattern of the $La_{0.85}PO_4Eu_{0.15}{}^{3+}$ nanorod sample. The right inset shows the proposed model of the monoclinic cell of the monazite crystal structure of $LaPO_4$ where an Eu atom replaces a La atom, and the left inset exhibits typical photographs of a brass metal circular holder filled with $La_{0.85}PO_4Eu_{0.15}{}^{3+}$ nanorod powder sample under room light as well as a 254 nm UV lamp (strong red emission of Eu^{3+} appears). (b) FTIR spectrum, (c) Raman spectrum, and (d) XPS survey scan spectrum of $La_{0.85}PO_4Eu_{0.15}{}^{3+}$ nanorods.

Information). These images clearly show the similar structure sustained after the hydroxide changes into the phosphate phase. We have varied the pH value from 9 to 11 and found pH ~11 produces nanorods with greater length. Thus, a plausible mechanism for nucleation of the nanorod structure depends upon the pH value of the metal complex precursor. The resultant solid material was filtered out and washed with distilled water followed by alcohol and then dried for 16 h. The doping amount of Eu^{3+} ($x = 0.05$–0.5) ions was varied in order to attain the optimum dopant concentration for the strongest red emission, which was measured by photoluminescence (PL) spectroscopic techniques. The PL intensity changes in accord with the different concentrations of Eu^{3+} (see details in Figure S5a in the Supporting Information). The concentration of europium in $La_{1-x}PO_4Eu_x{}^{3+}$ varied from $x = 0.05$ to $x = 0.5$; $x = 0.15$ ($La_{0.85}PO_4Eu_{0.15}{}^{3+}$) was found to be the optimum value for the synthesis of high-quality nanorods with high brightness. The sintering temperature for the synthesis of nanorods has also been optimized (see details in Figure S5b in the Supporting Information), where the maximum PL intensity for the $La_{0.85}PO_4Eu_{0.15}{}^{3+}$ nanorod sample was obtained at 800 °C. Then, the dried solid powder was heated at a slow heating rate of 5 °C min^{-1} to a set temperature of 800 ± 1 °C in a box furnace and maintained for 3 h in an air atmosphere. After completion of the reaction, the quartz crucible was found to be filled with a white granular mass, which was then easily crushed into a fine powder. In this method, the yield of material was more than 90% with a high degree of homogeneity throughout the mass. The versatility of this method is such that one can easily synthesize large quantities of homogeneous rare earth doped nanophosphors with a narrow size distribution.[47]

2.2. Characterization of $La_{1-x}PO_4$:$Eu_x{}^{3+}$ Nanorods.

Phase identification and gross structural analysis were performed by X-ray diffraction (XRD, Rigaku Cu $K\alpha_1$; $\lambda = 1.5406$ Å) techniques. Raman spectra were obtained using a Renishaw InVia Raman spectrometer with an excitation source of 514.5 nm. FTIR spectroscopic measurements were performed on a Thermo Scientific FTIR spectrometer (Nicolet Model 6700). Spectra were collected at a resolution of 2 cm^{-1}, and each spectrum was an average of 32 scans. The XPS analysis was performed in an ultrahigh-vacuum (UHV) chamber equipped with a hemispherical electron energy analyzer (PerkinElmer, PHI1257) using a nonmonochromated Al $K\alpha$ source (excitation energy of 1486.7 eV) with a base pressure of 4×10^{-10} Torr at room temperature. The surface morphology and microstructural characterization were determined by scanning electron microscopy (SEM, EVO MA 10 VPSEM) and high-resolution transmission electron microscopy (HRTEM, Technai Model No. G20-twin, 200kv with super twin lenses having point and line resolutions of 0.144 and 0.232 nm, respectively) equipped with energy dispersive X-ray analysis (EDAX) facilities for elemental studies. UV–visible spectra were collected using a high-resolution UV–vis spectrophotometer (Model No LS 55). Luminescence characterization was carried out using an Edinburgh luminescence spectrometer (Model No. F 900), and time-resolved spectroscopy (TRPL) was performed with an Edinburgh TRPL instrument (Model No. FLSP900), where a xenon lamp was used as the source of excitation. The PL mapping of luminescent nanorods was performed using a WITech alpha 300R+ confocal PL microscope system, where a 375 nm diode laser acted as a source of excitation.

2.3. Designing of Invisible Ink for Security.

A standard commercially available PVC gold medium (locally fabricated printing ink manufactured by Commercial Techno Colors, Ram Nagar, Varanasi, Uttar Pradesh, India) was used to disperse the as-synthesized $La_{0.85}PO_4Eu_{0.15}{}^{3+}$ nanorods for making invisible security ink. The

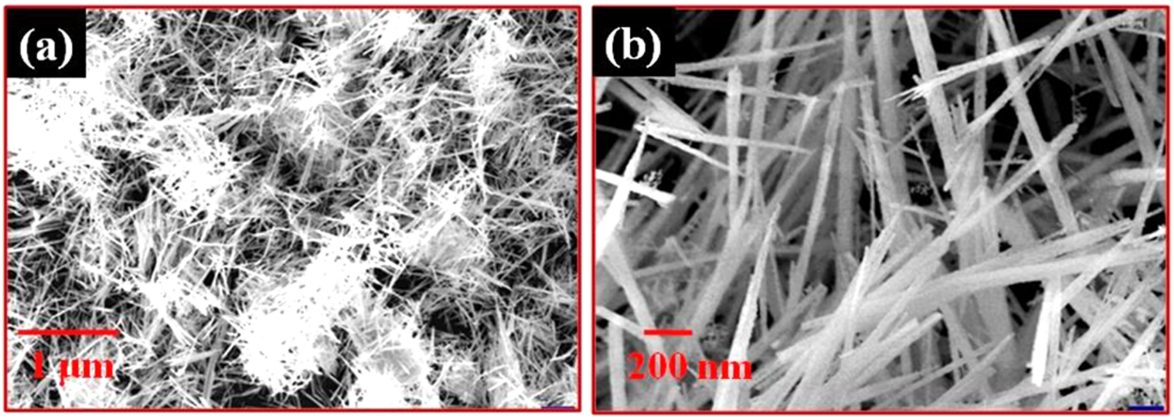

Figure 2. (a) SEM image of an $La_{0.85}PO_4Eu_{0.15}{}^{3+}$ nanorod sample and (b) magnified view of the nanorods.

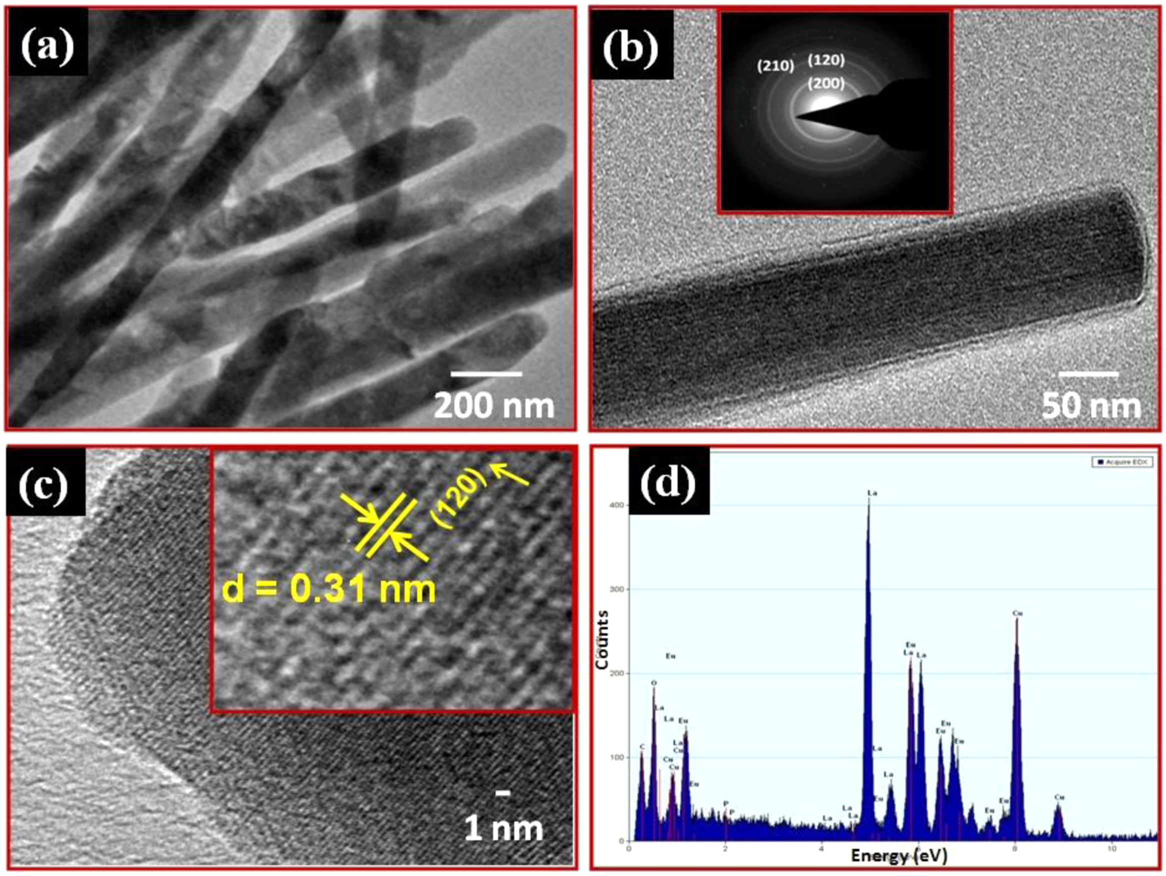

Figure 3. (a) TEM image exhibiting a bundle of nanorods. (b) Magnified view of single nanorods, with an inset showing the SAED pattern. (c) HRTEM image and (d) EDX pattern of a $La_{0.85}PO_4Eu_{0.15}{}^{3+}$ nanorod sample.

choice of dispersive medium is important due to two major facts: first for dispersal of rare earth species into the medium without formation of clusters or agglomerates of nanorods and second for efficient printing the viscosity of the medium (~3000 micropoise) is essential, which provides adhesive nature with printing paper. In a typical experiment, 175 mg of $La_{0.85}PO_4Eu_{0.15}{}^{3+}$ nanorods was mixed with 25 mL of a commercially purchased PVC gold medium solution. The resultant mixture was sonicated at 25 kHz frequency for 45 min to obtain a proper dispersion. A highly transparent (~88%) colloidal solution was obtained, which is further shown in Figure S6 (see the Supporting Information). To make an alphabet as a security pattern onto both art and pastel black paper, we used a standard screen printing technique for alphabet printing.

2.4. Biocompatibility. The cells were cultured and maintained in Dulbecco's Modified Eagle's Medium (DMEM) high glucose medium (Invitrogen) containing 4.5 g/L D-glucose, 4 mM L-glutamine, and 110 mg/L sodium pyruvate, supplemented with 10% fetal bovine serum (FBS), 100 IU mL^{-1} penicillin, and 100 μg mL^{-1} streptomycin in a humidified incubator at 37 °C with 5% CO_2. Each well of a 96-well cell culture plate was plated with 4×10^3 cells in 100 μL of the culture medium. After overnight culturing, the medium was replaced with a culture medium containing $La_{0.85}PO_4{:}Eu_{0.15}{}^{3+}$ nanophosphors in different concentrations ranging from 0 to 25 μg/mL in triplicate. After 24 and 48 h of incubation, the medium containing $La_{0.85}PO_4{:}Eu_{0.15}{}^{3+}$ nanophosphors was removed, and the cells were washed gently with 500 μL of warm, sterile phosphate buffer solution (PBS). To each well was added 200 μL of MTT reagent (0.5 mg/mL

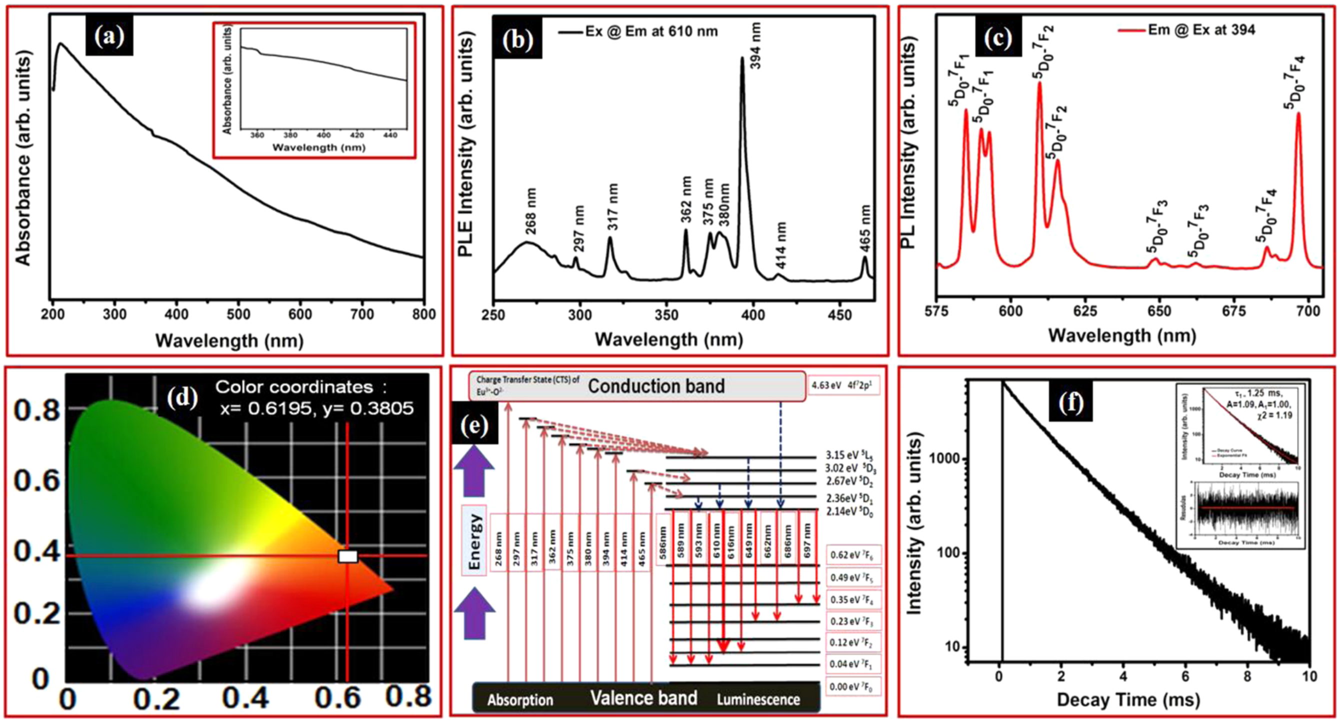

Figure 4. (a) Absorbance spectrum of $La_{0.85}PO_4Eu_{0.15}{}^{3+}$ nanorods in water dispersed medium. (b) PL excitation spectrum recorded at 610 nm emission wavelength. (c) PL emission spectrum obtained at 394 nm excitation showing a sharp, intense, hypersensitive red emission peak with maximum at 610 nm ($^5D_0$−$^7F_2$) at room temperature. (d) CIE chromaticity diagram showing the color coordinates for red color perception of the emission; x = 0.6195, y = 0.3805. (e) TRPL decay profile recorded at room temperature while monitoring the emission at 610 nm at an excitation wavelength of 394 nm. (f) Lifetime data and the parameter generated by the exponential fitting of $La_{0.85}PO_4Eu_{0.15}{}^{3+}$ nanorods.

in medium), and the plate was returned to the incubator for 4 h. After incubation, the medium with MTT reagent was removed and 200 μL of DMSO was added to each well. The cells were subsequently incubated for 5 min, and the optical densities of th esolubilized formazan salts were assessed at 570 nm with a Tecan Infinite M200 microplate reader (Mannedorf, Switzerland).

2.5. In Vitro Bioimaging. The cells were cultured and maintained in DMEM medium as described above. For bioimaging, 1 × 10^4 cells were plated in each well of a 4 well sterile chamber slides (Nunc, USA) with 500 μL culture medium. After overnight culture, 10 μg/mL $La_{0.85}PO_4$:$Eu_{0.15}{}^{3+}$was added to the culture medium and incubated in regular cell culture conditions. After both 4 and 24 h of culture, the medium with $La_{0.85}PO_4$:$Eu_{0.15}{}^{3+}$ nanophosphors was removed from the cells and washed two times with 1 mL phosphate buffer. Cells were fixed using 1% paraformaldehyde and mounted with Vectashield antifade mountingmedia with 4′-6-Diamidino-2-phenylindole (DAPI, Vector Laboratories, Inc., CA). Cellular imaging was done using a Nikon Eclipse 90i microscope equipped with the Cool SNaP HQ2 CCD camera (Photometrics, AZ). Nikon Intensilight C-HGFI lamp was used as the fluorescence light source.

3. RESULTS AND DISCUSSION

3.1. XRD, Raman, FTIR, and XPS Characterizations.

The as-synthesized white porous fluffy mass with a high degree of homogeneity was characterized through X-ray diffraction to confirm the phase purity of sample and gross structural analysis. Prior to the XRD measurements, calibration of the diffractometer was achieved with silicon powder (d_{111} = 3.1353 Å).[48] Figure 1a shows the XRD pattern of as-synthesized $La_{0.85}PO_4Eu_{0.15}{}^{3+}$ nanorods. The diffraction peaks are identified to be $LaPO_4$ crystalline phase with a monazite structure (space group $P2_1/n$) in the monoclinic system (JCPDS card no. 83-0651). Moreover, no diffraction peak corresponding to impurity ion is detected. The lattice parameters for all the variant $La_{1-x}PO_4Eu_x{}^{3+}$ nanorods (x = 0.05−0.5) were calculated from the observed D values through a least-squares fitting method using computer program based unit cell refinement software.[9] The unit cell volume is calculated for variants ($La_{1-x}PO_4Eu_x{}^{3+}$) from the observed lattice parameters and is shown in Table S2 (see the Supporting Information). It was noted that the cell parameter and cell volume increase for an Eu^{3+} doping concentration up to a value of 0.15 and then after this it started to decrease. The left inset of Figure 1a shows typical photographs of pellets of as-synthesized $La_{0.85}PO_4Eu_{0.15}{}^{3+}$ nanorods under room light as well as a 254 nm UV lamp (evidence of a strong red emission of Eu^{3+} under UV excitation). The right inset of Figure 1a shows the proposed model of the monoclinic cell of the monazite structure of $LaPO_4$.

FTIR analysis was carried out to determine the vibrational and rotational motion of the molecule. The FTIR spectrum of $La_{0.85}PO_4Eu_{0.15}{}^{3+}$ nanorods is shown in Figure 1b. The characteristic three bands located at 424, 546, and 622 cm^{-1} correspond to the bending vibrations (v_4 region), and the four peaks at 914, 1094, 1289, and 1405 cm^{-1} are attributed to the stretching vibrations (v_3 region) of the $PO_4{}^{3-}$ group. These vibration regions ofthe phosphate group confirm the monoclinic phase formation of lanthanum phosphate. The Raman scattering is very sensitive in determining the crystallinity and microstructure of the materials. It was employed to confirm the formation of the Eu^{3+}-doped $LaPO_4$ monoclinic phase and the existence of Eu ions on the surface of the $La_{0.85}PO_4Eu_{0.15}{}^{3+}$ nanorod sample. The Raman spectrum of $La_{0.85}PO_4Eu_{0.15}{}^{3+}$ nanorods is shown in Figure 1c. It shows that the Raman peaks at 335, 404, 475, 538, 556, 930, and 1045

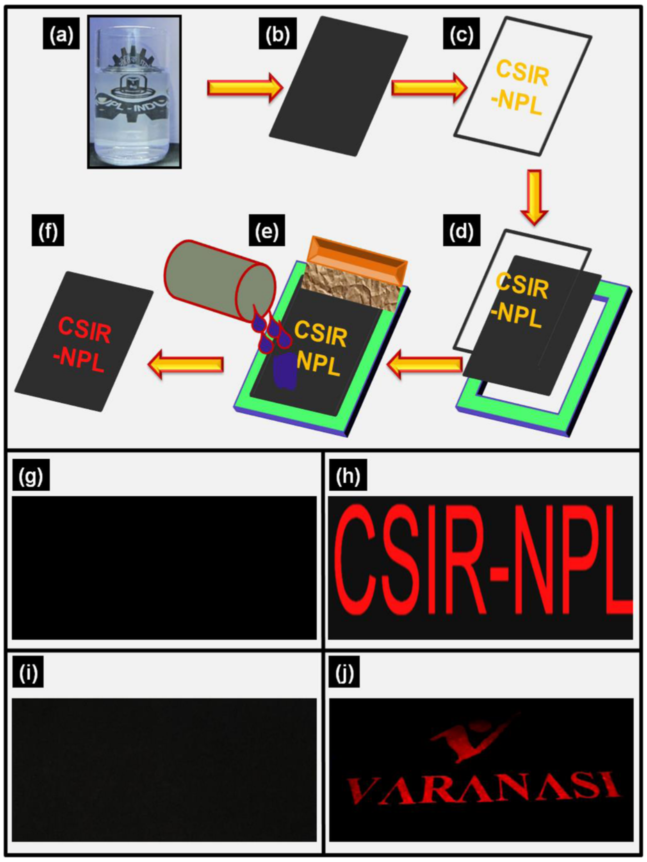

Figure 5. (a−f) Various steps involved in the systematic process for screen printing on black paper. (g, h) Shining art black paper screen printed CSIR-NPL alphabet which is obtained using a screen printing process technique and similarly (i, j) rough pastel black paper screen printed VARANASI alphabet. It can be easily seen that the images in (h) and (j) show the clear red emission printed alphabet which has been designed using $La_{0.85}PO_4:Eu_{0.15}^{3+}$ nanorods with PVC gold medium luminescent ink exhibiting hypersensitive red emission on excitation with a 254 nm UV lamp.

cm^{-1} correspond to the modes of the monoclinic phase of $LaPO_4$, respectively, which are consistent with the XRD results.

The chemical composition and formation of the $La_{0.85}PO_4Eu_{0.15}^{3+}$ nanorod sample were derived from XPS studies. Figure 1d shows a binding energy survey scan which was recorded with a pass energy of 100 eV. Binding energies are calibrated against the binding energy of the C(1s) peak at 284.6 eV. The XPS spectrum specifies the presence of La, Eu, P, and O elements in $La_{0.85}PO_4Eu_{0.15}^{3+}$ nanorods. It can be seen that the phosphorus significantly exists in the form of PO_4^{3+} groups in accord with its P(2s) binding energy located at 191.6 eV. The core level spectra of P(2s), La(3d), and Eu(3d) can also be clearly seen in Figure S7 (see the Supporting Information). The P(2s), La(3d), and Eu(3d) core level peaks were recorded using a pass energy of 35 eV.

3.2. Surface Morphology and Microstructural Characterizations. A typical scanning electron microscope (SEM) image of the optimum $La_{0.85}PO_4Eu_{0.15}^{3+}$ nanorod sample and a magnified view of select nanorods are shown in parts a and b of Figure 2, respectively. The sample clearly exhibits uniform nanorod-like structures with an average diameter of ∼90 nm and length of ∼2 μm. The observation of weakly bounded nanorods may be attributed to the fact that the rods have the tendency to agglomerate due to their high surface energy. Hence, these could be easily redispersed by ultrasonication in ethanol medium for ∼10 min.

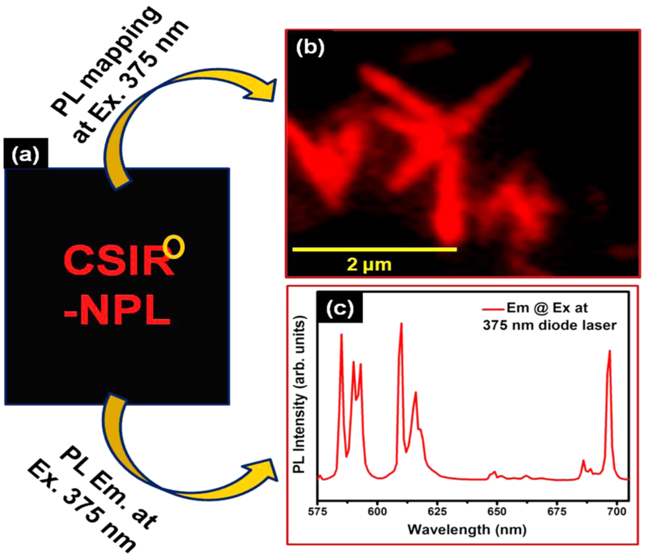

Figure 6. (a) Screen-printed red luminescent CSIR-NPL alphabet which was designed using $La_{0.85}PO_4:Eu_{0.15}^{3+}$ nanorods with PVC gold medium luminescent ink. (b) PL mapping of the particular area which is marked with a yellow circle in (a) at 375 nm wavelength excitation. (c) Corresponding PL spectrum.

To examine the individual structures of nanorods and to find out more details about the atomic lattice arrangement, we performed transmission electron microscopy (TEM) and high-resolution transmission electron microscopy (HRTEM). For better TEM images, the $La_{0.85}PO_4Eu_{0.15}^{3+}$ nanorod powder sample was dispersed in ethanol medium for 10 min and a drop was placed on the surface of the carbon-coated grid and allowed to dry before TEM imaging. The TEM image of the $La_{0.85}PO_4Eu_{0.15}^{3+}$ nanorod sample and a magnified view of a single nanorod are shown in parts a and b of Figure 3, respectively. The TEM image clearly depicts the formation of nanorods of average diameter lying in the range 80−90 nm. The selected area electronic diffraction (SAED) pattern of the $La_{0.85}PO_4Eu_{0.15}^{3+}$ nanorod sample is shown in the inset of Figure 3b. It is consistent with high crystallinity and order in crystallography. The diffraction spots could be indexed as a monoclinic phase with lattice planes (200), (120), and (210). These are in good agreement with the results of XRD. A typical HRTEM image of a $La_{0.85}PO_4Eu_{0.15}^{3+}$ nanorod sample is shown in Figure 3c. The precise observation of the HRTEM image indicates that the sample exhibits lattice fringes with an estimated interspacing of 0.31 nm, corresponding to the (120) plane of $La_{0.85}PO_4Eu_{0.15}^{3+}$ nanorods with a monazite phase of the monoclinic system. The growth orientation plane of nanorods in the HRTEM image is denoted by yellow arrows, which is in good agreement with the obtained XRD results. The clear and damage-free lattice fringes are easily observed, which reveal a good crystal quality with minimal lattice fringe distortion. Qualitative elemental analysis of synthesized nanorods was performed using EDAX, as shown in Figure 3d. It exhibits the presence of europium, lanthanum, phosphorus, and oxygen elements in the $La_{0.85}PO_4Eu_{0.15}^{3+}$ nanorod sample.

3.3. UV−Visible, PL, and TRPL Spectroscopy. UV−visible spectra were collected using a high-resolution UV−vis spectrophotometer through quartz cells with a 10 mm path length, as shown in Figure 4a. The absorbance spectrum of the

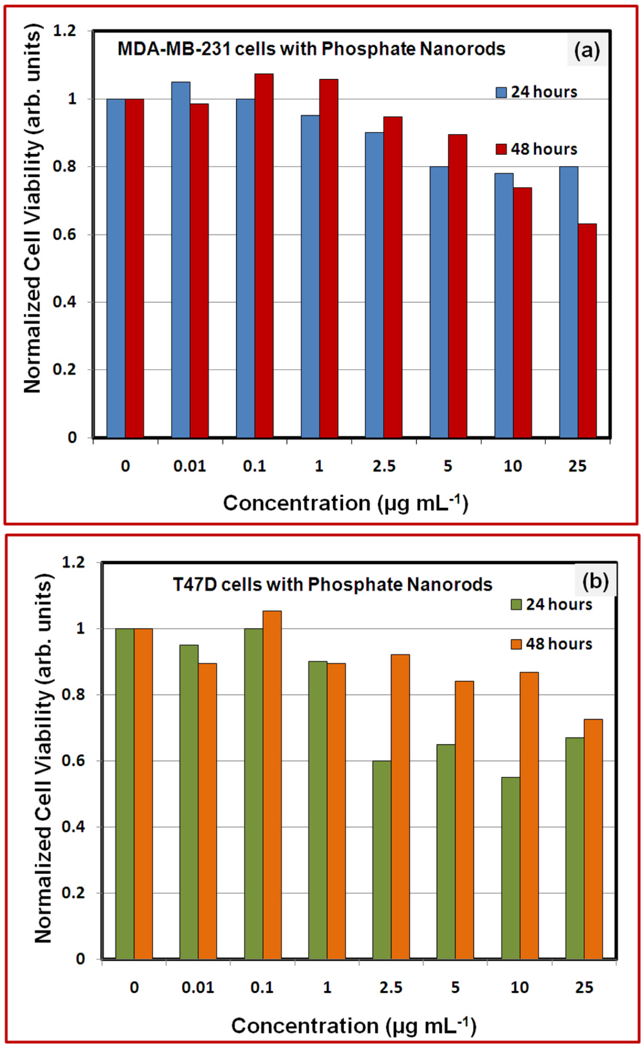

Figure 7. Normalized cell viability assay with human breast cancer cell lines, (a) MDA-MB-231 and (b) T47D, incubated with different concentrations of $La_{0.85}PO_4$:$Eu_{0.15}{}^{3+}$ nanorods for different incubation time periods (24 and 48 h).

$La_{0.85}PO_4Eu_{0.15}{}^{3+}$ nanorod sample was investigated from a solution of the nanorods dispersed in water. This spectrum contains several transitions with a strong peak at 212 nm. This is ascribed to the absorption due to charge transfer states (CTS) of O−Eu. A very weak shoulder originating from the Eu^{3+} f−f transitions is also observed in the 300−400 nm region, which is in agreement with the PL excitation spectrum. The enlarged view from 340 to 450 nm is shown in the inset of Figure 4a. The transmittance spectrum of the $La_{0.85}PO_4Eu_{0.15}{}^{3+}$ nanorod sample is shown in Figure S6 (see the Supporting Information). The sample is highly transparent (∼88%) in the visible range, which contributes to the formation of scattering free/less luminescent layers.

In order to optimize the PL intensity and high brightness of the $La_{1-x}PO_4Eu_x{}^{3+}$ nanorods for maximum efficiency, the concentration of europium in the nanorods was varied from x = 0.05 to x = 0.5. It has been observed that x = 0.15 (15 mol %) is optimum for the synthesis of nanorods with high-intensity photoluminescence with good brightness, as confirmed through Figure S5a (see the Supporting Information), which shows that initially there is a steady increase in PL with an increase in europium concentration up to x = 0.15. However, beyond this optimum value, the intensity started to decrease rapidly and sharply, which may be attributed to luminescence quenching owing to excess Eu^{3+} ions. It is well-known that the doping concentration of europium can affect the distance between two Eu^{3+} ions in the host lattice. When the europium concentration is ≤15 mol %, the two Eu^{3+} ions are far apart and each one of the Eu^{3+} ions can be regarded as an isolated luminescent center, which independently emits light without any interference. On the other hand, nearby Eu^{3+} ions mutually interact by an electric multipolar process due to the shortened distances between two Eu^{3+} ions at a high doping concentration of more than 15 mol %. In the latter case, the energy transfer rates of Eu^{3+} ions easily exceed the radiative rates. Thus, the absorbed photon energy rapidly migrates among Eu^{3+} ions in the host lattice, which can decrease the probabilities of the radiative transitions of Eu^{3+}ions and even quench the fluorescence if the excited state gets trapped in an energy sink with a high nonradiative deactivation rate constant.

Figure 4b exhibits the excitation spectrum for the $La_{0.85}PO_4Eu_{0.15}{}^{3+}$ nanorod sample, obtained by monitoring the strongest emission of the Eu^{3+} ions at 610 nm fixed wavelength. The broad absorption band at about 268 nm in the spectra originates from the Eu−O CTS, which occurs by electron delocalization from the filled 2p shell of the O^{2-} to the partially filled 4f shell of Eu^{3+}. In the long-wavelength region (300−500 nm), the f−f transitions within the Eu^{3+} $^4F_6$ electron configuration is also observed. These sharp peaks correspond to the direct excitation of Eu^{3+} from the ground state into higher energy levels arising from the 4f manifold, and the $^7F_0$−$^5L_6$ transition at 394 nm in particular has a greater contribution to the Eu^{3+} emission than the CTS transition at 268 nm. The PL emission spectrum for the $La_{0.85}PO_4Eu_{0.15}{}^{3+}$ nanorod sample recorded at 394 nm excitation wavelength is shown in Figure 4c. It depicts a sharp intense hypersensitive red emission at 610 nm wavelength. The four emission regions 580−600, 600−630, 640−660, and 680−700 nm are ascribed to the $^5D_0$−$^7F_1$, $^5D_0$−$^7F_2$, $^5D_0$−$^7F_3$, and $^5D_0$−$^7F_4$ radiative transitions, respectively. According to the PL intensities, the splitting of subpeaks at 586, 589, and 593 nm from the $^5D_0$−$^7F_1$ transition (I_m), the splitting subpeak at 610 and 616 nm from the $^5D_0$−$^7F_2$ transition (I_e), splitting subpeaks at 649 and 662 nm from the $^5D_0$−$^7F_3$ transition (I_m), and the splitting subpeaks at 686 and 697 nm from the $^5D_0$−$^7F_4$ transition (I_m) are observed. As is well known, the $^5D_0$−$^7F_1$, $^5D_0$−$^7F_3$, and $^5D_0$−$^7F_4$ lines appear from magnetic dipole transitions, while the $^5D\_$-$^7F_2$ lines are generated from electric dipole transitions. The other emission spectra at the different excitation wavelengths 268, 297, 317, 362, 375, 380, 394, 414, and 465 nm are shown in Figure S8 (see the Supporting Information) and gave a maximum emission at 394 nm excitation, which represents the best excitation wavelength for the highest emission. It has also been observed that $LaPO_4$ has higher luminescence in comparison to corresponding family members such as $GdPO_4$, $CePO_4$, $NdPO_4$, $SmPO_4$, $TbPO_4$, and YPO_4 (see details in Figure S9 in the Supporting Information). The estimated color coordinates of red emission at x = 0.6195, y = 0.3805 for the $La_{0.85}PO_4Eu_{0.15}{}^{3+}$ nanorod sample is shown in Figure 4d. The complete excitation and emission mechanism involved in the process is shown schematically in Figure 4e (energy level diagram). It represents the charge transfer between Eu^{3+} and O^{2-}. The cooperatively excited Eu^{3+} ions in the $^5D_2$ level, due to the contribution of the O^{2-} ion pair through CET (cooperative energy transfer), give strong red emissions. The

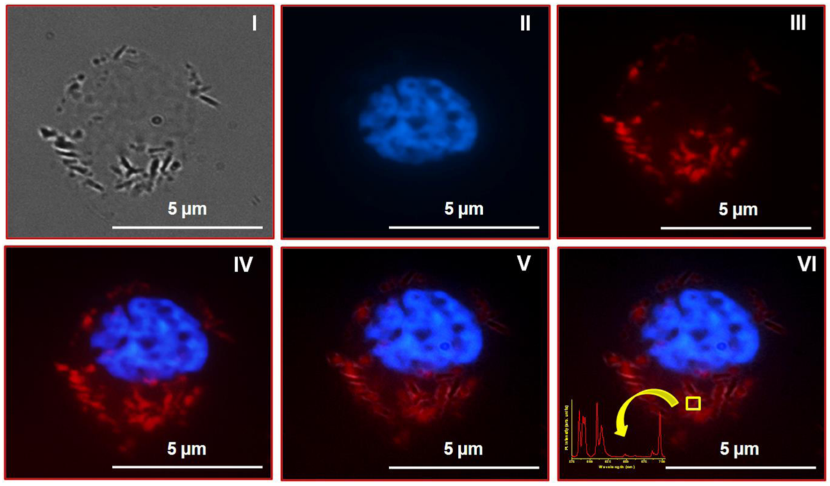

Figure 8. In vitro fluorescence microscopy images of T47D cells incubated with $La_{0.85}PO_4:Eu_{0.15}{}^{3+}$ nanorods (10 μg mL^{-1}) for 4 h. Sequential images show (I) phase contrast of T47D cells, (II) an individual nucleus stained blue with 4′,6-diamidino-2-phenylindole (DAPI), (III) red fluorescence staining by $La_{0.85}PO_4:Eu_{0.15}{}^{3+}$ nanorods, (IV) overlapped images of blue DAPI and red $La_{0.85}PO_4:Eu_{0.15}{}^{3+}$ nanorods, (V) overlap of phase contrast, blue and red, from I−III, respectively, and (VI) in vitro localized PL images of $La_{0.85}PO_4:Eu_{0.15}{}^{3+}$ nanorods from V. Inset: localized PL spectrum taken from level cells (red).

exciton lifetime is a dependent parameter with respect to the size and shape of the crystal, which can be studied using time-resolved photoluminescence spectroscopy (TRPL). The efficiency of the radiative recombination is directly proportional to the decay time of the particular transition. Figure 4f shows the luminescence decay profile of the $La_{0.85}PO_4Eu_{0.15}{}^{3+}$ nanorod sample. The decay was recorded for the Eu^{3+} transition at 610 nm emission with 394 nm excitation wavelength measured at room temperature by a time-correlated single photon counting technique. The lifetime data of $^5D_0$−$^7F_2$ (610 nm) transitions of Eu^{3+} in $La_{0.85}PO_4Eu_{0.15}{}^{3+}$ were very well fitted to a single-exponential function as $I(t) = A + A_1 \exp(-t/\tau_1)$, where τ_1 is the decay lifetime of the luminescence, A_1 is the weighting parameter, and A is constant. The fitting curve with generated parameters is given in the inset of Figure 4f. The observed lifetime is $\tau_1 \approx 1.25$ ms. Thus, the time-resolved spectroscopy results indicate that the as-synthesized $La_{0.85}PO_4Eu_{0.15}{}^{3+}$ nanorods are highly suitable for security ink and bioimaging applications.[49−51]

3.4. Strategic Applications of $La_{0.85}PO_4Eu_{0.15}{}^{3+}$ Nanorods.

To explore the feasibility of luminescent $La_{0.85}PO_4Eu_{0.15}{}^{3+}$ nanorods for its potential applications, proposed areas are discussed and described below.

3.4.1. Security Ink Applications: $La_{0.85}PO_4Eu_{0.15}{}^{3+}$ Nanorods for Invisible Security Codes. Lanthanide phosphate based colloid can be applied as an indispensable and consequential craft to make highly stable security ink for security code applications. For this, we have synthesized luminescent ink from $La_{0.85}PO_4:Eu_{0.15}{}^{3+}$ nanorods sample by dispersing the powder sample in a commercially available PVC gold medium (details are described in the Experimental Section). Recently, we have established the use of PVC gold medium in rare earth oxide nanorods ($Y_2O_3:Er^{3+}/Yb^{3+}$ nanorods) to fabricate the luminescent ink in anticounterfeiting applications.[45] The stability of the ink (luminescent colloid) was strongly affected by the mixing process of the powder and the solvent. The PVC gold medium is easily available commercially, having a low cost, high stability, and sticky nature. Hence, it was required that the mixing process must be performed for a time duration of 45 min at room temperature to produce transparent stable colloids (Figure S10a (see Supporting Information)), which is desired for our security ink applications. The process demonstrates the transparency of colloid solutions of nanorods under room light with good stability for several hours. When we excite the colloidal suspension of nanorods in PVC gold medium with 254 nm excitation from a UV hand lamp, a strong red emission peaking at 610 nm is exhibited, as shown in Figure S10b (see Supporting Information). The screen printing test was performed on black paper to show the potential use of the colloidal solution for making security codes. A transparent solution of $La_{0.85}PO_4:Eu_{0.15}{}^{3+}$ nanorods with PVC gold medium as a luminescent ink, black paper, and CSIR-NPL alphabets printed mesh (printed at the Advertising and Communication Printing Agency, Maldahiya, Varanasi, Uttar Pradesh, India) were used for the printing process (Figure 5a−c). The printed mesh was fixed in the frame with black paper (Figure 5d). The luminescent ink was poured onto the mesh, and a squeegee was moved across the surface of the mesh (Figure 5e). Thus, we obtained the screen-printed CSIR-NPL alphabets on black paper after removal of the mesh from the frame and excitation (Figure 5f). This clearly demonstrates the hypersensitive red color of screen-printed alphabets after UV 254 nm wavelength excitation, which legitimizes its potential applications as an invisible security ink to print security codes. The schematic diagram of screen printing on a black paper is shown in Figure 5a−f. In order to examine the efficient screen printing process, we have used two types of black papers: (i) art black paper and (ii) pastel black paper. The art black paper (commercial name) is smooth and shining black in nature. This kind of paper provides a more efficient screen printing image, which can be clearly seen in Figure 5g,h. The pastel black paper has a rougher surface with a dull sheen. This kind of paper provides a roughly textured screen printing image which can be clearly seen in Figure 5i,j. In Figure 5h,j, the printed alphabets based on $La_{0.85}PO_4:Eu_{0.15}{}^{3+}$ nanorod assisted PVC gold medium luminescent ink exhibit hypersensitive red emission after 254 nm UV lamp excitation.

Furthermore, we examined the fluorescent mapping and their corresponding PL emission spectrum of selected areas of a screen-printed luminescent CSIR-NPL alphabet (Figure 6a) to confirm the distribution of $La_{0.85}PO_4$:$Eu_{0.15}^{3+}$ nanorods with PVC gold medium. Figure 6b exhibits the PL mapping of the particular area which is marked with a yellow circle at 375 nm excitation wavelength, and Figure 6c depicts the corresponding PL spectrum. We have also taken SEM and optical images of the $La_{0.85}PO_4$:$Eu_{0.15}^{3+}$ nanorod sample dispersion into PVC gold medium at selected areas of screen-printed luminescent CSIR-NPL alphabet (Figure 6a), as shown in Figures S11 and S12 (see the Supporting Information), respectively.

3.4.2. High-Contrast Bioimaging Application: Biocompatible $La_{0.85}PO_4Eu_{0.15}^{3+}$ Nanorods for in Vitro Bioimaging. Lanthanide-derived phosphors can also be adapted as fluorescent labels of molecules, which is a standard technique in biology for the sensitive detection of proteins and nucleic acids in time-resolved fluorometric assays and in immunoassays. Cellular permeability and cytotoxicity features of fluorescent nanomaterials are critical to their application as luminescent biological labels. The labels are often organic dyes or organic phosphors that give rise to the usual problems of broad spectral features, short lifetime, photobleaching, and potential toxicity to cells. Alternative labels may be based on lanthanide-derived phosphors. It has already been demonstrated that inorganic fluorescent lanthanides such as europium and terbium orthophosphate (e.g., $EuPO_4 \cdot H_2O$ and $TbPO_4 \cdot H_2O$) nanorods can behave as biolabels and can be internalized into human umbilical vein endothelial cells, 786-O cells, or renal carcinoma cells, though the exact mechanism for their internalization remains unclear.[52,53] These can offer the potentially significant advantage of a relatively long lived emission, as it is free of problems related to quenching. In addition, the emission is well-separated from the background emission that appears in environmental and biological samples. As $La_{0.85}PO_4$:$Eu_{0.15}^{3+}$ nanorods retain their desirable optical properties and exhibit a spectrally intense, narrow, red emission with addition of an enhanced fluorescence lifetime (1.25 ms for 0.15% Eu^{3+} concentration), their application as labels in immunoassay yield a very good emission.

Prior to performing the cytotoxicity test of $La_{0.85}PO_4Eu_{0.15}^{3+}$ nanorods for breast cancer cells, we have dispersed $La_{0.85}PO_4Eu_{0.15}^{3+}$ nanorods in deionized water to examine the stability of colloidal suspension of nanorods in water without any ligands. A 2 mg portion of $La_{0.85}PO_4Eu_{0.15}^{3+}$ nanorod powder was dispersed in 20 mL of DI water, and the mixture was sonicated (ultrasonicated bath) for 30 min at 25 kHz frequency to observe the stability of a colloidal suspension of $La_{0.85}PO_4Eu_{0.15}^{3+}$ of nanorods in DI water. After sonication, the colloidal suspension was kept for 12 h and we found that the colloidal suspension was stable for 12 h without settling of the nanorods at bottom of the vial, which can be seen clearly in Figure S13a,b (see the Supporting Information).

To examine whether the $La_{0.85}PO_4Eu_{0.15}^{3+}$ nanorod sample is biocompatible, we performed the standard MTT (3-(4,5-dimethylthiazol-2-yl)-2,5-diphenyltetrazolium bromide) assay to determine the cytotoxicity of $La_{0.85}PO_4Eu_{0.15}^{3+}$ nanorods in two different human breast cancer cell lines (MDA-MB-231 and T47D) for specific incubation periods (24 and 48 h). The normalized data of the cell viability assay with human breast cancer cell lines (MDA-MB-231 and T47D) incubated with different concentrations of $La_{0.85}PO_4$:$Eu_{0.15}^{3+}$ nanorods for different incubation periods (24 and 48 h) are given in Figure 7. It can be seen from Figure 7 that up to 1 μg mL^{-1} there is no major cellular growth inhibition observed with these nanorods in both cancerous cells lines for 48 h. Cells incubated in growth medium without any $La_{0.85}PO_4Eu_{0.15}^{3+}$ nanorods were used as controls to investigate cell growth (labeled as concentration 0 in Figure 7). The cell viability analysis for MDA-MB-231 after treatment with different concentrations of the anticancer drug doxorubicin as a positive control for the MTT assay has been previously reported in our earlier studies.[8] Furthermore, to investigate whether $La_{0.85}PO_4$:$Eu_{0.15}^{3+}$ nanorods can be used for cellular imaging, we performed in vitro cellular studies using human breast cancer cell lines T47D (Figure 8). Figure 8 represents the fluorescence microscopy images of T47D cells treated with $La_{0.85}PO_4Eu_{0.15}^{3+}$ nanorods for 4 h. The cellular nucleus is stained blue by DAPI, and the intense hypersensitive red fluorescent $La_{0.85}PO_4Eu_{0.15}^{3+}$ nanorod molecules are distributed throughout the cytoplasm, as shown in Figure 8I–V. The overlap of fluorescence and phase contrast images clearly shows the cell-specific cellular localization of $La_{0.85}PO_4Eu_{0.15}^{3+}$ nanorods. In vitro fluorescence microscopy for negative control images of T47D cells without treatment with nanophosphor (10 μg mL^{-1}) are shown in Figure S14 (see the Supporting Information). The localized PL emission spectrum acquired from the cells showed the characteristic PL of Eu^{3+} peaking at 610 nm (inset of Figure 8VI). The complete absence of autofluorescence confirms the capability of $La_{0.85}PO_4Eu_{0.15}^{3+}$ nanorods for high-contrast PL imaging of cells in vitro. Therefore, the blue color of the nucleus (DAPI) and strong red color clearly show the potential use of nanorods for high-contrast bioimaging applications.

4. CONCLUSION

We have successfully synthesized highly luminescent europium-doped lanthanum orthophosphate nanorods with 1.25 ms photoluminescence lifetime using a facile customized chemical precipitation method. The XRD pattern reveals the crystalline phase of $La_{0.85}PO_4Eu_{0.15}^{3+}$ nanorods, assigned to a monazite-type structure in a monoclinic system. SEM and TEM images indicate the nanorod-like structure with an average diameter of ~90 nm and length of ~2 μm. The nanorods have colloidal stability and optical transparency in commercially available PVC gold medium, highly efficient hypersensitive red emission with characteristically sharp spectral lines in the visible region, and low cellular toxicity. Thus, this simple and effective approach provides excellent highly luminescent $La_{0.85}PO_4Eu_{0.15}^{3+}$ nanorods for security inks and in vitro high-contrast bioimaging applications.

■ ASSOCIATED CONTENT

Ⓢ Supporting Information

Further details of $La_{0.85}PO_4$:$Eu_{0.15}^{3+}$ nanorods, as given in Figures S1–S11 and Tables S1 and S2 (described in the text). This material is available free of charge via the Internet at http://pubs.acs.org.

■ AUTHOR INFORMATION

Corresponding Author

*E-mail for B.K.G.: bipinbhu@yahoo.com.

Present Address

○Department of Physics, Kalindi College, University of Delhi, New Delhi, India.

Author Contributions

#These authors contributed equally.

Notes

The authors declare no competing financial interest.

■ ACKNOWLEDGMENTS

The authors wish to thank Prof. R. C. Budhani, Director, NPL, New Delhi, India, for his keen interest in this work. The authors are grateful to Prof. O. N. Srivastava (Banaras Hindu University, Varanasi) for his encouragement. The authors gratefully acknowledge financial support from the University Grant Commission (UGC), Government of India, and the DLD Cancer Center, Baylor College of Medicine Pilot Project. The authors are grateful to the CSIR-NPL TAPSUN program, providing a PL mapping facility.

■ REFERENCES

(1) Alivisatos, A. P. *Science* **1996**, *271*, 933−937.
(2) Murray, C. B.; Kagan, C. R. *Annu. Rev. Mater. Sci.* **2000**, *30*, 545−610.
(3) Hu, J. T.; Odom, T. W.; Lieber, C. M. *Acc. Chem. Res.* **1999**, *32*, 435−445.
(4) Murphy, C. J.; Jana, N. R. *Adv. Mater.* **2002**, *14*, 80−82.
(5) Xia, Y.; Yang, P.; Sun, Y.; Wu, Y.; Mayers, B.; Gates, B.; Yin, Y.; Kim, F.; Yan, H. *Adv. Mater.* **2003**, *15*, 353−389.
(6) Patzke, G. R.; Krumeich, F.; Nesper, R. *Angew. Chem., Int. Ed.* **2002**, *41*, 2446−2461.
(7) Gupta, B. K.; Rathee, V.; Narayanan, T. N.; Thanikaivelan, P.; Saha, A.; Thanikaivelan, T. N.; Saha, P.; Govind, A.; Shanker, V.; Marti, A. A.; Ajayan, P. M. *Small* **2011**, *7*, 1767−1773.
(8) Gupta, B. K.; Narayanan, T. N.; Vithayathil, S. A.; Lee, Y.; Koshy, S.; Reddy, A. L. M.; Saha, A.; Shanker, V.; Singh, V. N.; Kaipparettu, B. A.; Marti, A. A.; Ajayan, P. M. *Small* **2012**, *7*, 1−7.
(9) Gupta, B. K.; Haranath, D.; Saini, S.; Singh, V. N.; Shanker, V. *Nanotechnology* **2010**, *21*, 055607.
(10) Kan, S.; Mokari, T.; Rothenberg, E. *Nat. Mater.* **2003**, *2*, 155−158.
(11) Reich, D. H.; Tanase, M.; Hultgren, A.; Bauer, L. A.; Chen, C. S.; Meyer, G. J. *J. Appl. Phys.* **2003**, *93*, 7275−7280.
(12) Dexpert-Ghys, J.; Mauricot, R.; Faucher, M. D. *J. Lumin.* **1996**, *69*, 203−215.
(13) Singh, L. R.; Ningthoujam, R. S.; Sudarsan, V.; Srivastava, I.; Singh, S. D.; Dey, G. K.; Kulshreshtha, S. K. *Nanotechnology* **2008**, *19*, 055201.
(14) Palilla, F. C.; Levine, A. K. *Appl. Opt.* **1966**, *5*, 1467−1468.
(15) Singh, N. S.; Ningthoujam, R. S.; Devi, L. R.; Yaiphaba, N.; Sudarsan, V.; Singh, S. D.; Vatsa, R. K.; Tewari, R. *J. Appl. Phys.* **2008**, *104*, 104307.
(16) Singh, N. S.; Ningthoujam, R. S.; Yaiphaba, N.; Singh, S. D.; Vatsa, R. K. *J. Appl. Phys.* **2009**, *105*, 064303.
(17) Ningthoujam, R. S.; Shukla, R.; Vatsa, R. K.; Duppel, V.; Kienle, L.; Tyagi, A. K. *J. Appl. Phys.* **2009**, *105*, 084304.
(18) Ningthoujam, R. S.; Sudarsan, V.; Godbole, S. V.; Kienle, L.; Kulshreshtha, S. K.; Tyagi, A. K. *Appl. Phys. Lett.* **2007**, *90*, 173113.
(19) Rao, C. M.; Sudarsan, V.; Ningthoujam, R. S.; Gautam, U. K.; Vatsa, R. K.; Vinu, A.; Tyagi, A. K. *J. Nanosci. Nanotechnol.* **2008**, *8*, 5776−5780.
(20) Yaiphaba, N.; Ningthoujam, R. S.; Singh, N. S.; Vatsa, R. K.; Singh, N. R. *J. Lumin.* **2010**, *130*, 174−180.
(21) Srinivasu, K.; Ningthoujam, R. S.; Sudarsan, V.; Vatsa, R. K.; Tyagi, A. K.; Srinivasu, P.; Vinu, A. *J. Nanosci. Nanotechnol.* **2009**, *9*, 3034−3039.
(22) Ferhi, M.; Horchani-Naifer, K.; Ferid, M. *J. Rare Earths* **2009**, *27*, 182−186.
(23) Anitha, M.; Ramakrishnan, P.; Chatterjee, A.; Alexander, G.; Singh, H. *Appl. Phys. A: Mater. Sci. Process.* **2002**, *74*, 153−162.
(24) Kar, A.; Datta, A.; Patra, A. *J. Mater. Chem.* **2010**, *20*, 916−922.
(25) Ghosh, P.; Olivia, J.; De La Rosa, E.; Haldar, K. K.; Solis, D.; Patra, A. *J. Phys. Chem. C* **2008**, *112*, 9650−9658.
(26) Zhu, L.; Liu, X.; Liu, X.; Li, Q.; Li, J.; Zhang, S.; Meng, J.; Cao, X. *Nanotechnology* **2006**, *17*, 4217−4222.
(27) Wang, F.; Xue, X.; Liu, X. *Angew. Chem., Int. Ed.* **2008**, *47*, 906−909.
(28) Li, C.; Yang, J.; Quan, Z.; Yang, P.; Kong, D.; Lin, J. *Chem. Mater.* **2007**, *19*, 4933−4942.
(29) Bai, X.; Song, H.; Pan, G.; Lei, Y.; Wang, T.; Ren, X.; Lu, S.; Dong, B.; Dai, Q.; Fan, L. *J. Phys. Chem. C* **2007**, *111*, 13611−13617.
(30) Yi, G. S.; Chow, G. M. *Chem. Mater.* **2007**, *19*, 341−343.
(31) Choi, C. L.; Koski, K. J.; Olson, A. C. K.; Alivisatos, A. P. *Proc. Natl. Acad. Sci. U.S.A.* **2010**, *107*, 21306−21310.
(32) Schrier, J.; Demchenko, D. O.; Wang, L. W.; Alivisatos, A. P. *Nano Lett.* **2007**, *7*, 2377−2382.
(33) Park, H. G.; Barrelet, C. J.; Wu, Y.; Tian, B.; Qian, F.; Lieber, C. M. *Nat. Photonics* **2008**, *2*, 622−626.
(34) Chen, K.; Mirkin, C. A.; Lo, R. K.; Zhao, J.; McDevitt, J. T. *J. Am. Chem. Soc.* **1995**, *117*, 6374−6375.
(35) Gao, X.; Nie, S. *Mol. Biol.* **2005**, *303*, 61−71.
(36) Yan, H.; He, R.; Johnson, J.; Law, M.; Saykally, R. J.; Yang, P. *J. Am. Chem. Soc.* **2003**, *125*, 4728−4729.
(37) Patra, C. R.; Alexandra, G.; Patra, S.; Jacob, D. S.; Gedanken, A.; Landau, A.; Gofer, Y. *New. J. Chem.* **2005**, *29*, 733−739.
(38) Yu, L.; Song, H.; Lu, S.; Liu, Z.; Yang, L.; Kong, X. *J. Phys. Chem. B* **2004**, *108*, 16697−16702.
(39) Photon International, March 2005, 74.
(40) Heer, S.; Lehmann, O.; Haase, M.; Gudel, H. U. *Angew. Chem., Int. Ed.* **2003**, *42*, 3179−3182.
(41) Yu, L.; Song, H.; Lu, S.; Liu, Z.; Yang, L.; Kong, X. *J. Phys. Chem. B* **2004**, *108*, 16697−10702.
(42) Liu, X.; Wang, Q.; Gao, Z.; Sun, J.; Shen, J. *Cryst. Growth Design* **2009**, *9*, 3707−3713.
(43) Meruga, J. M.; Baride, A.; Cross, W.; Kellar, J. J.; Stanley, P. *J. Mater. Chem. C* **2014**, *2*, 2221−2227.
(44) Liu, Y.; Ai, K.; Lu, L. *Nanoscale* **2011**, *3*, 4804−4810.
(45) Kumar, P.; Dwivedi, J.; Gupta, B. K. *J. Mater. Chem. C* **2014**, *2*, 10468−10475.
(46) Zhang, F.; Wong, S. S. *ACS Nano* **2010**, *4*, 99−112.
(47) Li, L.; Su, Y.; Li, G. *J. Mater. Chem.* **2010**, *20*, 459−465.
(48) Kedawat, G.; Srivastava, S.; Jain, V. K.; Pawan; Kataria, V.; Agrawal, Y.; Vijay, Y. K. *ACS Appl. Mater. Interfaces* **2013**, *5*, 4872−4877.
(49) Shockley, W.; Queisser, H. J. *J. Appl. Phys.* **1961**, *32*, 510.
(50) Shalav, A.; Richards, B. S.; Trupke, T.; Kramer, K. W.; Gudel, H. U. *Appl. Phys. Lett.* **2005**, *86*, 013505.
(51) Shalav, A.; Richards, B. S.; Kramer, K.; Gudel, G. *Proc. 31st IEEE Photovolt. Specialists Conf.* **2005**, 114−117.
(52) Patra, C. R.; Bhattacharya, R.; Patra, S.; Basu, S.; Mukherjee, P.; Mukhopadhyay, D. *J. Nanobiotechnol.* **2006**, *4*, 1−15.
(53) Patra, C. R.; Bhattacharya, R.; Patra, S.; Basu, S.; Mukherjee, P.; Mukhopadhyay, D. *Clin. Chem.* **2007**, *53*, 2029−2031.